# Geophysical Research Letters

**Key Points:**
- When reaching geospace, magnetic clouds modify significantly the properties of the first geophysical region they encounter, the foreshock
- Typical quasi-monochromatic foreshock waves are replaced by a superposition of waves at different periods with a shorter transverse extent
- Multiple field-aligned beams observed during one event suggest a link between the multiple wave periods and the suprathermal ion properties

# First Observations of the Disruption of the Earth's Foreshock Wave Field During Magnetic Clouds

L. Turc[1] , O. W. Roberts[2,3], M. O. Archer[4] , M. Palmroth[1,5] , M. Battarbee[1] , T. Brito[1] , U. Ganse[1] , M. Grandin[1] , Y. Pfau-Kempf[1] ,C. P. Escoubet[3], and I. Dandouras[6]

[1]Department of Physics, University of Helsinki, Helsinki, Finland, [2]Space Research Institute, Austrian Academy of Sciences, Graz, Austria, [3]Directorate of Science, European Space Research and Technology Centre (ESA/ESTEC), Noordwijk, The Netherlands, [4]School of Physics and Astronomy, Queen Mary University of London, London, UK, [5]Finnish Meteorological Institute, Helsinki, Finland, [6]IRAP, Université de Toulouse/CNRS/UPS/CNES, Toulouse, France

**Abstract** The foreshock, extending upstream of Earth's bow shock, is a region of intense electromagnetic wave activity and nonlinear phenomena, which can have global effects on geospace. It is also the first geophysical region encountered by solar wind disturbances journeying toward Earth. Here, we present the first observations of considerable modifications of the foreshock wave field during extreme events of solar origin called magnetic clouds. Cluster's multispacecraft data reveal that the typical quasi-monochromatic foreshock waves can be completely replaced by a superposition of waves each with shorter correlation lengths. Global numerical simulations further confirm that the foreshock wave field is more intricate and organized at smaller scales. Ion measurements suggest that changes in shock-reflected particle properties may cause these modifications of the wave field. This state of the foreshock is encountered only during extreme events at Earth, but intense magnetic fields are typical close to the Sun or other stars.

**Plain Language Summary** Solar storms are giant clouds of particles ejected from the Sun into space during solar eruptions. When solar storms are directed toward Earth, they can cause large disturbances in near-Earth space, for example, disrupting communications or damaging spacecraft electronics. Understanding in detail what happens when solar storms reach Earth is crucial to mitigate their effects. Using measurements from the Cluster spacecraft, we investigate how solar storms modify the properties of the very first region of near-Earth space they encounter when journeying toward Earth. This region, called the foreshock, extends ahead of the protective bubble formed by the Earth's magnetic field, the magnetosphere. The foreshock is home to intense electromagnetic waves, and disturbances in this region can perturb the Earth's magnetosphere. Our study reveals that solar storms modify profoundly the foreshock, resulting in a more complex wave activity. Global numerical simulations performed with the Vlasiator code confirm our findings. These changes could affect the regions of space closer to Earth, for example, in modifying the wave properties or the amount of solar particles entering the Earth's magnetosphere. This needs to be taken into account to better anticipate the effects of solar storms at Earth.

## 1. Introduction

Magnetic clouds are strongly geoeffective solar transients, characterized by an enhanced and smoothly rotating magnetic field (Huttunen et al., 2005; Yermolaev et al., 2012). Understanding the details of their interaction with near-Earth space is crucial to forecast accurately their space weather effects. On their earthward journey, the first geophysical region that incoming magnetic clouds encounter is the Earth's foreshock.

The foreshock extends upstream of the quasi-parallel sector of the Earth's bow shock, where the $\theta_{Bn}$ angle between the interplanetary magnetic field (IMF) and the shock normal is below ~45° (Eastwood, Lucek, et al., 2005). The foreshock is permeated with intense electromagnetic waves, generated through plasma instabilities triggered by shock-reflected particles (Eastwood, Lucek, et al., 2005; Wilson, 2016). Foreshock processes can have global effects on the Earth's magnetosphere, causing enhanced wave activity down to the Earth's surface (Bier et al., 2014), or triggering geoeffective fast magnetosheath jets (Plaschke et al., 2018). Changes in the foreshock properties can therefore significantly affect conditions throughout geospace.

The most common waves in the Earth's ion foreshock are the so-called 30-s waves (Eastwood et al., 2002), quasi-monochromatic magnetic field fluctuations at a period around 30 s, left handed in the spacecraft frame. Their wavelength is about 1 $R_E$ (1 Earth radius = 6,371 km), while their finite transverse extent ranges between 8 and 18 $R_E$ (Archer et al., 2005). Close to the wave vector direction, the wave front is essentially planar over several Earth radii, and the overall shape of the waves is approximately an oblate spheroid (Archer et al., 2005). They have been identified as fast magnetosonic waves propagating sunward in the plasma frame but advected earthward by the faster solar wind flow (Eastwood et al., 2005a). They are excited by back-streaming field-aligned beams (FABs) via the right-hand resonant ion-ion beam instability. The cyclotron resonance condition associated with this mode is

$$\omega = V_{\text{beam}} k_{\parallel} - \Omega_{\text{ci}} \tag{1}$$

where $V_{\text{beam}}$ is the beam velocity and $\Omega_{\text{ci}}$ the ion gyrofrequency. These waves are generated around the mode interaction point of the cyclotron resonance with the fast magnetosonic branch, which can be approximated here as $\omega = v_A k_{\parallel}$, where $v_A$ is the Alfvén velocity (e.g., Eastwood et al., 2005a).

In spacecraft measurements, these waves are not observed in conjunction with the FABs that generated them, but with intermediate, gyrating or gyrophase-bunched distributions (Eastwood et al., 2005a; Kempf et al., 2015). Measurements taken shortly before or after observing the foreshock waves have however brought quantitative evidence of a cyclotron resonance between FABs and waves (Eastwood, Lucek, et al., 2005, and references therein). These waves have been extensively studied since their discovery (Greenstadt et al., 1968; Eastwood et al., 2005a, 2005b; Palmroth et al., 2015), and it is well established that their period depends on the IMF strength and orientation (Le & Russell, 1996; Takahashi et al., 1984).

Even though magnetic clouds are the most geoeffective solar wind disturbances, there are no studies focusing on the foreshock properties during such events. Recent numerical simulations predict that an enhanced IMF strength, as is encountered during magnetic clouds, could strongly affect the foreshock wave properties and their large-scale structuring (Turc et al., 2018). These simulations were however limited to a single set of upstream conditions, warranting a more general observational investigation.

## 2. Event Identification

Observations of foreshock waves during magnetic clouds are rare, as these transients pass by Earth only about 2% of the time (Yermolaev et al., 2012), and Earth-orbiting spacecraft cross the foreshock only sporadically. In the early phase (2001–2005) of the Cluster mission (Escoubet et al., 2001), the spacecraft separations are similar to the wave characteristic sizes (a few hundred kilometers), which allows us to determine accurately the wave properties. Using the catalogue introduced in Turc et al. (2016), we identify events when Cluster observes foreshock waves during a magnetic cloud and divide them into 5-min intervals.

Foreshock fast magnetosonic waves are mostly transverse and propagate at a small angle relative to the magnetic field vector (Eastwood et al., 2005b). Measurements from Cluster's fluxgate magnetometer (Balogh et al., 1997) are projected onto a frame where one axis is parallel to the mean magnetic field during the 5-min interval and the two others are perpendicular to it, forming a right-handed triplet. Then we perform a wavelet transform on the perpendicular magnetic field components and calculate the wavelet phase difference, to check the wave polarization (Torrence & Compo, 1998). Intervals of steepened waves and discrete wave packets are visually identified and rejected.

In total, we find six magnetic clouds with observations of left-handed foreshock waves (see Table S1 in the supporting information). These observations take place several hours after the passage of the interplanetary shock preceding the magnetic cloud, when near-Earth space is embedded deep within the magnetic cloud, which dictates the upstream conditions for the foreshock to develop. These strongly differ from typical solar wind conditions, in particular, due to the clouds' large IMF strength.

## 3. Results

### 3.1. A More Intricate Form of Wave Activity

During most events, we find that the foreshock wave field departs significantly from its usual state. To facilitate the comparison, Figure 1 shows an example of typical foreshock waves on 18 February 2003 analyzed in previous studies (Archer et al., 2005; Hobara et al., 2007; Kis et al., 2007; left) together with representative
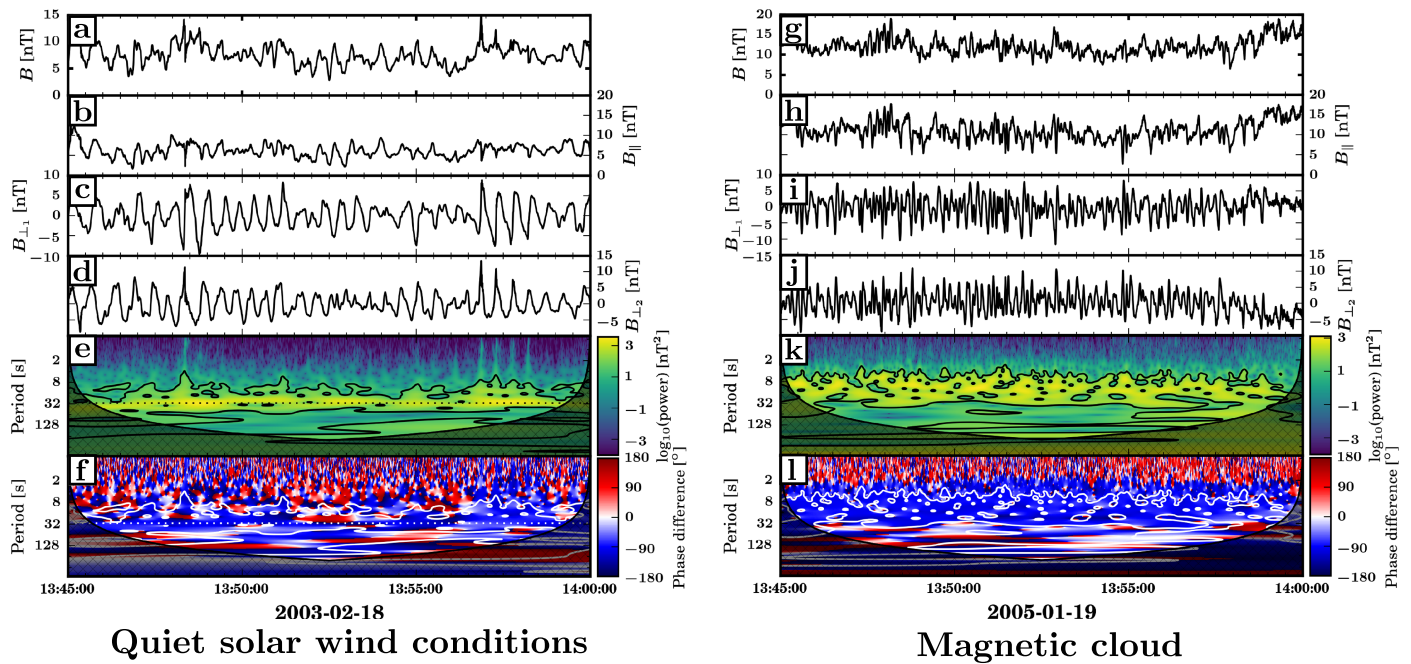
**Figure 1.** Foreshock waves on 18 February 2003 (left), during quiet solar wind conditions, and on 19 January 2005 (right), during a magnetic cloud. From top to bottom: magnetic field strength and components parallel and perpendicular to the mean magnetic field vector, wavelet power spectrum of $B_{\perp_1}$, and wavelet phase difference between $B_{\perp_1}$ and $B_{\perp_2}$. The dotted lines in panels e and f show the 30-s period. The black (white) contours in panels e and k (f and l) delineate the 95% significance level of the wavelet power spectrum. The hatched areas in panels e and f, and k and l show the cone of influence, where edge effects become significant in the wavelet spectrum.

observations during a magnetic cloud on 19 January 2005 (right). In both cases, foreshock waves appear as large-amplitude magnetic field oscillations, especially in the two perpendicular components (panels c and d, and i and j). During quiet conditions, the wavelet power spectrum showcases a rather narrow band of strong wave power around 30 s (panel e), while during magnetic clouds (panel k) high-fluctuation power is observed at periods between 5 and 30 s. The contours highlight where the wave power is strongest, showing that the fluctuations are left handed in the spacecraft frame (in blue in the phase difference plot, panel l).

Cluster's relative position in the foreshock can be determined from its measurements prior to the foreshock waves observations. Before 13:34 UT on 19 January 2005, Cluster was just outside the Earth's foreshock. The IMF rotation inside the magnetic cloud results in a progressive change of the $\theta_{Bn}$ angle along the field line connecting Cluster to the bow shock from 60° at 13:30 UT to 40° at 14:00 UT, according to a model bow shock (Jeřáb et al., 2005). Consequently, the spacecraft probe the outer foreshock, populated by FABs, from 13:34 UT, and then the foreshock wave field from 13:42 UT. In such a configuration, one would expect to observe the usual quasi-monochromatic fast magnetosonic waves. However, the power spectra of the left-handed foreshock waves display multiple spectral peaks whose periods vary with time (Figure 1k). This intricate spectrum is neither associated with right-handed polarization (in red in the phase difference plot) nor with highly steepened waves.

To identify the wave mode, we use two independent methods, multispacecraft timing analysis (Schwartz, 1998; applied to band-pass-filtered data to separate the different wave periods) and multipoint signal resonator (MSR; Narita et al., 2011; see supporting information). Their results for the first minutes of the data set are given in Table S2. The timing analysis yields wave vectors within 30° of the magnetic field. With the MSR technique, we find that the power distribution in wave vector space maximizes at two different wave vectors, showing the coexistence of two waves. The orientation of all wave vectors **k** toward $-x$ (i.e., earthward) and the negative wave velocities in the plasma frame $V_{\mathrm{wave,pl}}$ indicate that the waves propagate sunward in the plasma frame and are intrinsically right handed. This rules out 10-s Alfvén waves, intrinsically left handed (Eastwood et al., 2003). The Alfvén velocity was about $294 \pm 158$ km/s during this interval, the large uncertainties being due to large density fluctuations, as measured by the Cluster Ion Spectrometer (Rème et al., 2001). The estimated wave speeds are comparable to the Alfvén velocity, which is close to

the fast magnetosonic speed for large IMF strengths. These properties are all consistent with those of fast magnetosonic waves.

Both wave analysis techniques therefore consistently identify a superposition of fast magnetosonic waves at different periods, ranging between 6 and 17 s. These periods, lower than the usual 30 s, are due to the magnetic cloud's large IMF strength, here 11 nT, while its average value at Earth is about 5 nT. The frequency of foreshock fast magnetosonic waves changes with the IMF strength because their dispersion relation depends on this parameter, among others (Krauss-Varban et al., 1994). According to the Takahashi et al. (1984) empirical formula, the wave period should be 17 s under these solar wind conditions, very similar to the 18 s predicted by the Le and Russell (1996) formula, and consistent with the largest periods we observe. However, the lower wave periods are not accounted for by these models.

Similar intricate wavelet spectra are observed during four out of the six magnetic clouds under study (see the third column of Table S1). The waves were identified as fast magnetosonic waves during three of these events (22 January 2004, 19 January 2005, and 22 January 2005). For the last event, the wave mode could not be determined because of the extremely large IMF strength and solar wind velocity, resulting in the spacecraft tetrahedron being too large compared to the wavelength, making it impossible to identify uniquely the wave fronts.

The remaining two events display smoother wavelet spectra, as in normal solar wind conditions. The nature of the waves could not be confirmed during the 28 March 2001 event because of the poor correlation between the spacecraft time series, and of the large uncertainties in the flow velocity due to the very low density. Both events with smoother spectra were associated with much larger IMF cone angles (about 45°) than the more complex spectra (less than 30°), where the cone angle is measured between the IMF vector and the Sun-Earth line. Larger cone angles result in larger wave periods for a given IMF strength (Le & Russell, 1996; Takahashi et al., 1984), about 30 s on 23 April 2001. This suggests that the development of more complex foreshock wave activity is linked with shorter absolute wave periods.

### 3.2. A Possible Source for Multiple Fast Magnetosonic Waves

A recent numerical study also reported a superposition of fast magnetosonic waves in the foreshock associated with higher IMF strength (Turc et al., 2018). In the simulation, the multiple wave periods were attributed to ion velocity distribution functions (VDFs) with multiple FABs, instead of the single beam that usually generates quasi-monochromatic waves.

During all intervals under study, the ion VDFs have already evolved into intermediate and gyrating distributions when foreshock waves are observed, in agreement with previous works (e.g., Eastwood et al., 2005a). Cluster, however, probed the FAB region shortly before most of these intervals. We focus here only on those intervals for which fast magnetosonic waves were reliably identified (23 April 2001, 22 January 2004, 19 January 2005, and 22 January 2005). We checked that the upstream conditions remained essentially steady from the FAB observations to that of the waves, except for the IMF direction, which causes the foreshock wave field to reach the spacecraft. Based on the current understanding of foreshock wave generation, we can reasonably assume that the FABs we observe in the first place are representative of those generating the waves detected a few minutes later.

The upper part of Figure 2 displays representative VDFs recorded by the Hot Ion Analyzer instrument onboard Cluster-1 at 13:41:10 and 13:41:18 UT on 19 January 2005. The left column shows reduced two-dimensional (2-D) VDFs in the $(V_{\parallel}, V_{\perp})$ plane (relative to the magnetic field vector), integrated over the second perpendicular direction. In panels a and b, part of the solar wind population appears in red in the right-hand side, while backstreaming ions are in the left-hand side. The suprathermal population consists mostly of a FAB, centered at $V_{\parallel} \sim -1,500$ km/s. There is no clear evidence of multiple distinct FABs during this event, but a second population is observed at a nonzero pitch angle, centered around $V_{\perp} \simeq 1,000$ km/s. Panels c and d show the phase space density of the suprathermal population along a cut at $V_{\perp} = 0$. The beam shape is well fitted by a Gaussian (see also Table S3), most likely because the gyrating population is located at about the same $V_{\parallel}$ as the FAB. This second population appears as a second peak in phase space density on the cuts along $V_{\perp}$ at $V_{\parallel} = V_{\text{beam}}$ (panels e and f) and remain clearly visible for a range of $V_{\parallel}$ (not shown). The suprathermal population is better fitted by a sum of two Gaussians in these cuts (see Table S3), thus confirming that the two peaks are well distinct.
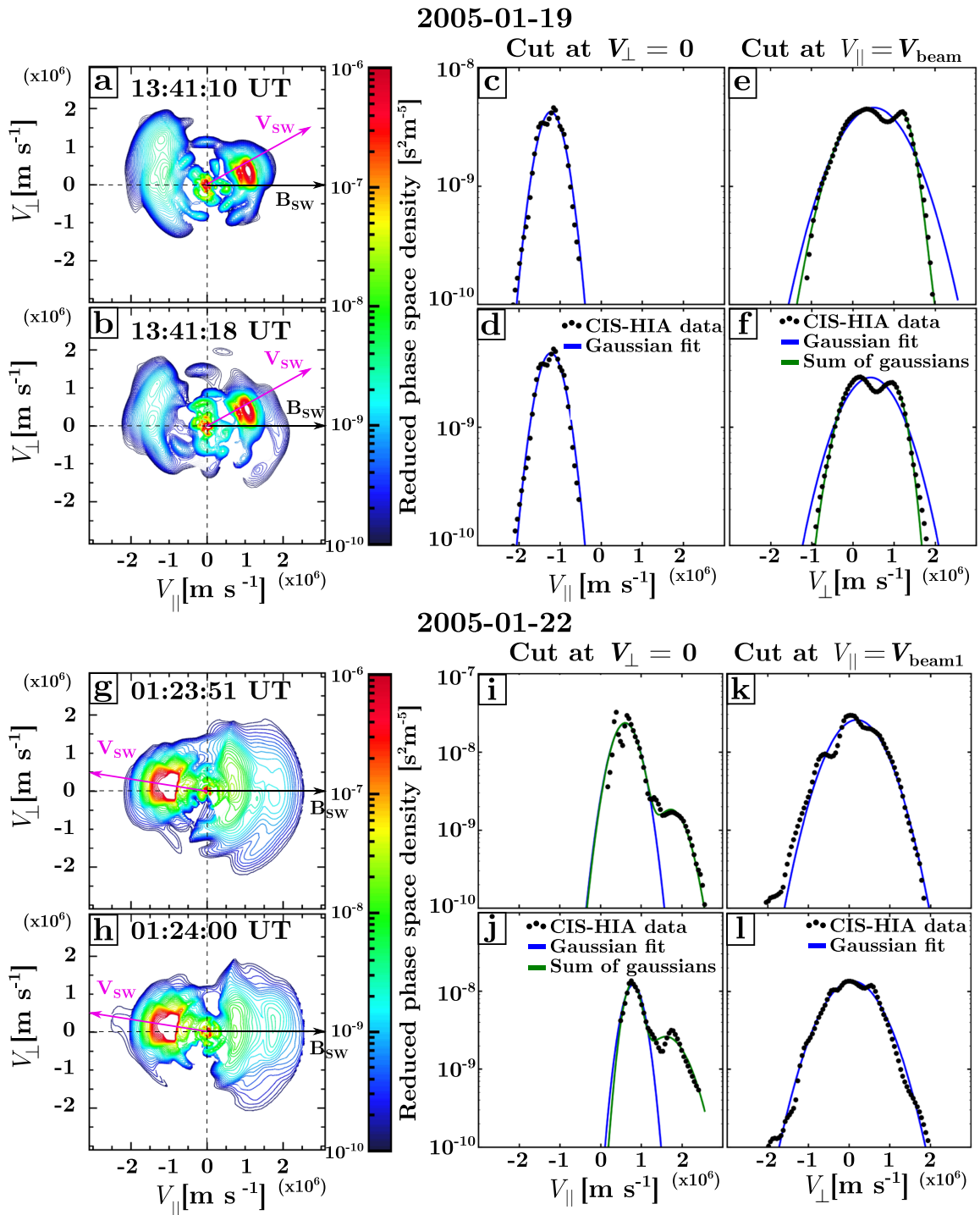
**Figure 2.** Ion VDFs observed shortly before the foreshock waves. (a–f) The 19 January 2005 event. (g–l) The 22 January 2005 event. Left column: reduced 2-D VDFs, integrated over the second perpendicular velocity direction. Color coded is the phase space density. The *x* and *y* axes are along and perpendicular to the magnetic field direction, respectively. Middle and right columns: cuts through the reduced distribution functions shown in the left column, at $V_\perp = 0$ (middle) and $V_\parallel = V_{beam}$ (right). VDF = velocity distribution function.

During the 23 April 2001 event, typical quasi-monochromatic foreshock waves were observed, accompanied with typical FABs. During the 22 January 2004 event, a sharp rotation of the IMF shortly before 12:00 UT causes a rapid motion of the foreshock boundary. Only two to three VDFs are recorded when Cluster crosses the FAB region. Given the rapid motion of the boundary, we cannot draw firm conclusions regarding the FABs during this event.

Finally, the 22 January 2005 event brings clear evidence of multiple FABs (Figure 2, bottom part) similar to those reported by Turc et al. (2018). Because of the different IMF orientation, the solar wind population in panels g and h is at negative $V_{\parallel}$ during this event. The FABs are centered around $V_{\parallel} \sim 700$ and $1{,}700$ km/s, respectively, and are well fitted by a sum of two Gaussians (panels i and j and Table S3). From these fits and Gaussian fits along $V_{\perp}$ at $V_{\parallel} = V_{\text{beam1}}$ (panels k and l) and $V_{\parallel} = V_{\text{beam2}}$, we estimate the temperature anisotropy (ratio of the perpendicular to parallel temperatures) of each of the beams (see Table S4). They range between 2 and 10, in excellent agreement with previous observations (Paschmann et al., 1981). The two FABs evolve progressively in consecutive VDFs for about a minute. At 01:24:00 UT, the higher-energy beam reaches its highest phase space density, peaking at about $4.1 \times 10^{-9}$ s$^2$/m$^5$, only a factor of 3 lower than the other beam, at about $1.3 \times 10^{-8}$ s$^2$/m$^5$.

To our knowledge, this is the first time that multiple FABs are observed in conjunction with unusual foreshock wave activity. Spacecraft observations of multiple FABs have been reported by Meziane et al. (2011) but were associated with typical quasi-monochromatic waves. The IMF strength was relatively high (9 nT) during the main interval analyzed in Meziane et al. (2011) but was not associated with a magnetic cloud. The comparison of the cyclotron resonant speed of the waves with that of the FABs revealed that only the main beam was in cyclotron resonance with the waves (Meziane et al., 2011).

The cyclotron resonant speed of the waves, normalized to the solar wind speed, is calculated as

$$P_{\text{res}} = \frac{\Omega_{\text{ci}} \cos \theta_{kV}}{\omega_{\text{sc}} \cos \theta_{kB}} \tag{2}$$

where $\omega_{\text{sc}}$ is the wave frequency in the spacecraft frame and $\theta_{kV}$ ($\theta_{kB}$) is the angle between the wave vector and the solar wind velocity vector (the IMF vector; Meziane et al., 2011). We calculate $P_{\text{res}}$ for the multiple FABs observed around 01:24 UT on 22 January 2005. We find that the velocity of the lower-energy beam normalized with the solar wind speed ranges between 1.8 and 1.9 and that of the higher-energy beam between 3.0 and 3.1. This is in excellent agreement with the cyclotron resonant speeds of the waves observed from 01:32 UT onward, which are 1.9 and 3.3.

### 3.3. Structuring of the Foreshock at Smaller Scales

During magnetic clouds, fast magnetosonic waves have shorter periods, which, in the plasma rest frame, translates into shorter wavelengths. Another critical parameter for the structuring of the foreshock wave field is the wave correlation length. This parameter can be estimated using cross correlations of measurements from pairs of spacecraft (see Archer et al., 2005, and supporting information). Here, we calculate the wave correlation length in the plane perpendicular to the wave vector. We divide all our intervals of fast magnetosonic waves into 120-s sections, so that for each interval the wave period and the upstream parameters remain roughly constant while retaining a sufficient number of wave periods. We obtain a reliable estimate of the transverse extent of the waves for 35 intervals, displayed as a histogram in Figure 3a. The transverse extent ranges between 1 and 10 R$_E$ (average 3.5 R$_E$; median 3.2 R$_E$). This is significantly shorter than during quiet solar wind conditions (8–18 R$_E$; Archer et al., 2005). Moreover, we find that the transverse extent of the waves is well correlated with the wave period, as evidenced by Figure 3b (correlation coefficient: 0.83), and we checked that this result is insensitive to the chosen interval length. This correlation implies that the waves retain the same aspect ratio when their wavelength varies; that is, the ratio of their wavelength over their transverse extent is roughly constant in the events under study.

To get a clearer view of the large-scale structuring of the foreshock, we use two global simulations performed with the hybrid-Vlasov Vlasiator code (Palmroth et al., 2018; von Alfthan et al., 2014), already studied in Turc et al. (2018). In both runs, the simulation domain is 2-D in real space, describing the equatorial plane of near-Earth space. The IMF has a 5° cone angle, the solar wind velocity is $\mathbf{V}_{\text{SW}} = (-600, 0, 0)$ km/s and the ion density $n_{\text{SW}} = 3.3$cm$^{-3}$. The IMF strength is set to 5 nT in Run 1, corresponding to regular IMF strength at Earth, and 10 nT in Run 2, comparable to the 19 January 2005 event.
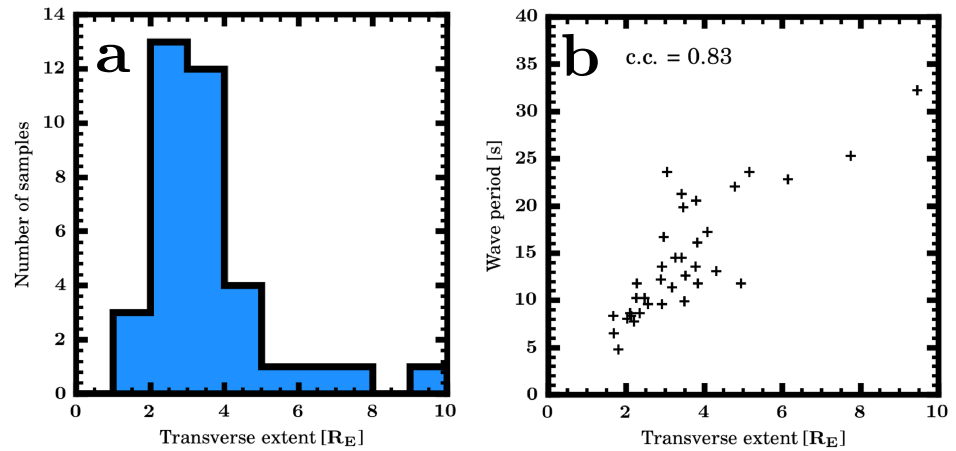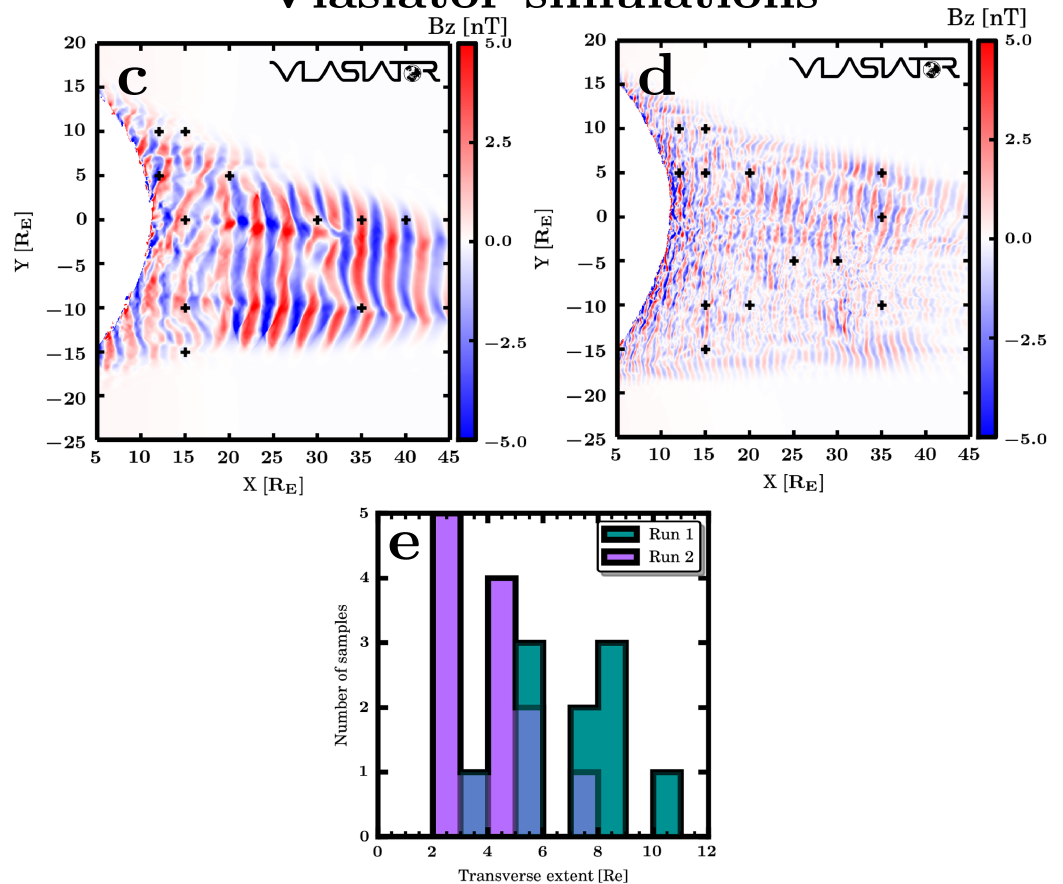
**Figure 3.** Transverse extent of the foreshock waves. Upper part: Cluster's observations during magnetic clouds. (a) Distribution of the transverse extent of foreshock waves. (b) Wave period as a function of the transverse extent. Bottom part: global simulations. (c and d) Magnetic field $B_z$ component in Runs 1 and 2 at time $t = 500$ s from the beginning of the runs, which illustrate the foreshock wave field. The plus signs indicate the positions of triplets of virtual spacecraft where the transverse extent of the wave fronts was reliably determined. (e) Distribution of the transverse extent of the wave fronts.

The out-of-plane ($B_z$) component of the magnetic field in the simulation domain is displayed in Figures 3c (Run 1) and 3d (Run 2). For clarity, the regions downstream of the bow shock are not shown. Because the foreshock waves are mostly transverse, $B_z$ is a good marker of the foreshock wave field. As can readily be seen from these plots, the waves are coherent over much larger scales during quiet solar wind conditions. The plus signs indicate the barycentric positions of triplets of virtual spacecraft, mimicking the Cluster constellation in 2-D, where the transverse extent of the waves was estimated reliably. Since the simulation is 2-D, only three spacecraft are needed to determine the wave properties. Magnetic field time series are extracted at each virtual spacecraft location and we estimate the transverse extent of the waves using the same cross-correlation technique as in Cluster data, albeit only with three spacecraft. The results of the analysis are shown as a histogram in panel e. The transverse extent of the waves varies significantly depending on the position in the foreshock. We obtain values ranging between 3 and 11 $R_E$ in Run 1 and between 2 and 6 $R_E$ in Run 2, the smallest values being encountered closer to the bow shock, especially in Run 1. The average (median) transverse extent of the waves is 7 (7.4) $R_E$ in Run 1 and 4 (4.3) $R_E$ in Run 2.

These results are in reasonable agreement with Cluster data, supporting the fact that the simulated foreshock wave field is representative of the actual foreshock. This suggests that during quiet solar wind conditions, the foreshock wave field is composed of large-scale coherent waves. When moving closer to the bow shock, their transverse extent decreases. At large IMF strength, as is the case during magnetic clouds, the correlation length of the waves becomes significantly shorter.

## 4. Discussion and Conclusions

We have presented the first observations of the Earth's foreshock during magnetic clouds, revealing that the foreshock develops during such events but its wave properties are strongly modified due to the unusual upstream conditions dictated by the clouds. Using multispacecraft analysis techniques, we show that the usually quasi-monochromatic fast magnetosonic waves are replaced by a superposition of waves at different periods. Their wavelength and their transverse extent are shorter, suggesting that the foreshock is structured over smaller scales.

Atypical ion VDFs are observed in conjunction with the unusual wave activity. During one event, we find clear evidence of two distinct FABs in cyclotron resonance with the waves observed shortly afterward, consistent with previous numerical works (Turc et al., 2018). In another, the FAB is accompanied by a second suprathermal population at nonzero pitch angle, which might have evolved from a second FAB, due to gyrophase trapping (Mazelle et al., 2003; Kempf et al., 2015). The apparent lack of multiple FABs during this event could also be due to the spacecraft connectivity to the bow shock. Using a model bow shock, we estimate that the observed FABs originate from $\theta_{Bn} \sim 52°$ during this event, and from $\theta_{Bn} \sim 43°$ when multiple FABs are observed on 19 January 2005 and in the Meziane et al. (2011) event. Local changes of the quasi-perpendicular shock geometry could generate multiple FABs (Meziane et al., 2011), since their energy depends on the local shock geometry upon their generation (Paschmann et al., 1980). Foreshock processes are a significant source of local shock deformations (Meziane et al., 2011). Therefore, the observations of multiple FABs being more likely at lower $\theta_{Bn}$ values, that is, closer to the foreshock, fits well within this scenario.

We note here that the second beam in the Meziane et al. (2011) event was not associated with intricate wave activity. Its maximum phase space density was about 2 orders of magnitude lower than that of the first beam, which could explain why it did not trigger additional fast magnetosonic waves. On the contrary, on 22 January 2005, the maximum phase space densities of the two beams only differ by a factor of 3, and both beams can thus generate fast magnetosonic waves of comparable amplitudes, as their growth rate increases with increasing beam density (Gary, 1991).

In this work, the wave properties have been determined assuming a linear picture, which remains appropriate here as the spectral peaks of the waves are well distinct. This allows separation of the different wave modes, as done previously in Hobara et al. (2007). Nonlinear wave analysis may be necessitated in other circumstances where distinct periodicities are not present.

Foreshock waves are known to modulate the shape of the shock front (Burgess, 1995). Therefore, their smaller wavelength and their smaller transverse extent during magnetic clouds could both result in smaller

ripples at the shock front, which in turn can affect particle reflection at the quasi-parallel bow shock (Wu et al., 2015) and the formation of magnetosheath high-speed jets (Plaschke et al., 2018).

IMF strengths above 10 nT are relatively uncommon at Earth, but they become typical closer to the Sun. At Mercury's orbit, the average IMF strength is about 20–30 nT (Korth et al., 2011). The small size of Mercury's magnetosphere results however in another organization of its foreshock wave field (Le et al., 2013). Outside of our solar system, exoplanets orbiting close to their host stars are immersed in intense magnetic fields and could thus display similar foreshock properties as presented here.

# References

Archer, M., Horbury, T. S., Lucek, E. A., Mazelle, C., Balogh, A., & Dandouras, I. (2005). Size and shape of ULF waves in the terrestrial foreshock. *Journal of Geophysical Research*, *110*, A05208. https://doi.org/10.1029/2004JA010791

Balogh, A., Dunlop, M. W., Cowley, S. W. H., Southwood, D. J., Thomlinson, J. G., Glassmeier, K. H., & Kivelson, M. G. (1997). The Cluster magnetic field investigation. *Space Science Reviews*, *79*, 65–91. https://doi.org/10.1023/A:1004970907748

Bier, E. A., Owusu, N., Engebretson, M. J., Posch, J. L., Lessard, M. R., & Pilipenko, V. A. (2014). Investigating the IMF cone angle control of Pc3-4 pulsations observed on the ground. *Journal of Geophysical Research: Space Physics*, *119*, 1797–1813. https://doi.org/10.1002/2013JA019637

Burgess, D. (1995). Foreshock-shock interaction at collisionless quasi-parallel shocks. *Advances in Space Research*, *15*, 159–169. https://doi.org/10.1016/0273-1177(94)00098-L

Capon, J. (1969). High resolution frequency-wavenumber spectrum analysis. In *Proceedings of the IEEE*, *57*, IEEE, pp. 1408–1418.

Eastwood, J. P., Balogh, A., Dunlop, M. W., Horbury, T. S., & Dandouras, I. (2002). Cluster observations of fast magnetosonic waves in the terrestrial foreshock. *Geophysical Research Letters*, *29*(22), e2046. https://doi.org/10.1029/2002GL015582

Eastwood, J. P., Balogh, A., Lucek, E. A., Mazelle, C., & Dandouras, I. (2003). On the existence of Alfvén waves in the terrestrial foreshock. *Annales Geophysicae*, *21*, 1457–1465. https://doi.org/10.5194/angeo-21-1457-2003

Eastwood, J. P., Balogh, A., Lucek, E. A., Mazelle, C., & Dandouras, I. (2005a). Quasi-monochromatic ULF foreshock waves as observed by the four-spacecraft Cluster mission: 1. Statistical properties. *Journal of Geophysical Research*, *110*, A11219. https://doi.org/10.1029/2004JA010617

Eastwood, J. P., Balogh, A., Lucek, E. A., Mazelle, C., & Dandouras, I. (2005b). Quasi-monochromatic ULF foreshock waves as observed by the four-spacecraft Cluster mission: 2. Oblique propagation. *Journal of Geophysical Research*, *110*, A11220. https://doi.org/10.1029/2004JA010618

Eastwood, J. P., Lucek, E. A., Mazelle, C., Meziane, K., Narita, Y., Pickett, J., & Treumann, R. A. (2005). The foreshock . *Space Science Reviews*, *118*, 41–94. https://doi.org/10.1007/s11214-005-3824-3

Escoubet, C. P., Fehringer, M., & Goldstein, M. (2001). Introduction the Cluster mission. *Annales Geophysicae*, *19*, 1197–1200. https://doi.org/10.5194/angeo-19-1197-2001

Gary, S. P. (1991). Electromagnetic ion/ion instabilities and their consequences in space plasmas—A review. *Space Science Reviews*, *56*, 373–415. https://doi.org/10.1007/BF00196632

Greenstadt, E. W., Green, I. M., Inouye, G. T., Hundhausen, A. J., Bame, S. J., & Strong, I. B. (1968). Correlated magnetic field and plasma observations of the Earth's bow shock. *Journal of Geophysical Research*, *73*, 51. https://doi.org/10.1029/JA073i001p00051

Hobara, Y., Walker, S. N., Balikhin, M., Pokhotelov, O. A., Dunlop, M., Nilsson, H., & Rème, H. (2007). Characteristics of terrestrial foreshock ULF waves: Cluster observations. *Journal of Geophysical Research*, *112*, A07202. https://doi.org/10.1029/2006JA012142

Huttunen, K. E. J., Schwenn, R., Bothmer, V., & Koskinen, H. E. J. (2005). Properties and geoeffectiveness of magnetic clouds in the rising, maximum and early declining phases of solar cycle 23. *Annales Geophysicae*, *23*, 625–641. https://doi.org/10.5194/angeo-23-625-2005

Jeřáb, M., Němeček, Z., ŠCSafránková, J., Jelínek, K., & Měerka, J. (2005). Improved bow shock model with dependence on the IMF strength. *Planetary and Space Science*, *53*, 85–93. https://doi.org/10.1016/j.pss.2004.09.032

Kempf, Y., Pokhotelov, D., Gutynska, O., Wilson III, L. B., Walsh, B. M., von Alfthan, S., & Palmroth, M. (2015). Ion distributions in the Earth's foreshock: Hybrid-Vlasov simulation and THEMIS observations. *Journal of Geophysical Research: Space Physics*, *120*, 3684–3701. https://doi.org/10.1002/2014JA020519

Kis, A., Scholer, M., Klecker, B., Kucharek, H., Lucek, E. A., & Rème, H. (2007). Scattering of field-aligned beam ions upstream of Earth's bow shock. *Annales Geophysicae*, *25*, 785–799. https://doi.org/10.5194/angeo-25-785-2007

Korth, H., Anderson, B. J., Zurbuchen, T. H., Slavin, J. A., Perri, S., Boardsen, S. A., & McNutt, R. L. (2011). The interplanetary magnetic field environment at Mercury's orbit . *Planetary and Space Science*, *59*, 2075–2085. https://doi.org/10.1016/j.pss.2010.10.014

Krauss-Varban, D., Omidi, N., & Quest, K. B. (1994). Mode properties of low-frequency waves: Kinetic theory versus Hall-MHD. *Journal of Geophysical Research*, *99*(A4), 5987–6010. https://doi.org/10.1029/93JA03202

Laakso, H., Perry, C., McCaffrey, S., Herment, D., Allen, A. J., Harvey, C. C., & Turner, R. (2010). Cluster active archive: Overview . *Astrophysics and Space Science Proceedings*, *11*, 3–37. https://doi.org/10.1007/978-90-481-3499-1_1

Le, G., Chi, P. J., Blanco-Cano, X., Boardsen, S., Slavin, J. A., Anderson, B. J., & Korth, H. (2013). Upstream ultra-low frequency waves in Mercury's foreshock region: MESSENGER magnetic field observations. *Journal of Geophysical Research: Space Physics*, *118*, 2809–2823. https://doi.org/10.1002/jgra.50342

Le, G., & Russell, C. T. (1996). Solar wind control of upstream wave frequency. *Journal of Geophysical Research*, *101*(A2), 2571–2576. https://doi.org/10.1029/95JA03151

Mazelle, C., Meziane, K., Le Quéau, D., Wilber, M., Eastwood, J. P., Rème, H., & Balogh, A. (2003). Production of gyrating ions from nonlinear wave-particle interaction upstream from the Earth's bow shock: A case study from Cluster- CIS. *Planetary and Space Science*, *51*, 785–795. https://doi.org/10.1016/j.pss.2003.05.002

Meziane, K., Hamza, A. M., Wilber, M., Mazelle, C., & Lee, M. A. (2011). Anomalous foreshock field-aligned beams observed by Cluster. *Annales Geophysicae*, *29*, 1967–1975. https://doi.org/10.5194/angeo-29-1967-2011

Narita, Y., Glassmeier, K. H., & Motschmann, U. (2011). High-resolution wave number spectrum using multi-point measurements in space—The Multi-point Signal Resonator (MSR) technique. *Annales Geophysicae*, *29*, 351–360. https://doi.org/10.5194/angeo-29-351-2011

Palmroth, M., Archer, M., Vainio, R., Hietala, H., Pfau-Kempf, Y., Hoilijoki, S., & Eastwood, J. P. (2015). ULF foreshock under radial IMF: THEMIS observations and global kinetic simulation Vlasiator results compared. *Journal of Geophysical Research: Space Physics*, *120*, 8782–8798. https://doi.org/10.1002/2015JA021526

Palmroth, M., Ganse, U., Pfau-Kempf, Y., Battarbee, M., Turc, L., Brito, T., & von Alfthan, S. (2018). Vlasov methods in space physics and astrophysics. *Living Reviews in Computational Astrophysics*, *4*, 1. https://doi.org/10.1007/s41115-018-0003-2

Paschmann, G., Sckopke, N., Asbridge, J. R., Bame, S. J., & Gosling, J. T. (1980). Energization of solar wind ions by reflection from the Earth's bow shock. *Journal of Geophysical Research*, *85*(A9), 4689–4694. https://doi.org/10.1029/JA085iA09p04689

Paschmann, G., Sckopke, N., Papamastorakis, I., Asbridge, J. R., Bame, S. J., & Gosling, J. T. (1981). Characteristics of reflected and diffuse ions upstream from the Earth's bow shock. *Journal of Geophysical Research*, *86*(A6), 4355–4364. https://doi.org/10.1029/JA086iA06p04355

Plaschke, F., Hietala, H., Archer, M., Blanco-Cano, X., Kajdič, P., Karlsson, T., & Sibeck, D. (2018). Jets downstream of collisionless shocks. *Space Science Reviews*, *214*(5), 4–81. https://doi.org/10.1007/s11214-018-0516-3

Rème, H., Aoustin, C., Bosqued, J. M., Dandouras, I., Lavraud, B., Sauvaud, J. A., & Sonnerup, B. (2001). First multispacecraft ion measurements in and near the Earth's magnetosphere with the identical Cluster ion spectrometry (CIS) experiment. *Annales Geophysicae*, *19*, 1303–1354. https://doi.org/10.5194/angeo-19-1303-2001

Schmidt, R. O. (1986). Multiple emitter location and signal parameter estimation. *IEEE Transactions on Antennas and Propagation*, *34*, 276–280. https://doi.org/10.1109/TAP.1986.1143830

Schwartz, S. J. (1998). Shock and discontinuity normals, Mach numbers, and related parameters. *ISSI Scientific Reports Series*, *1*, 249–270.

Takahashi, K., McPherron, R. L., & Terasawa, T. (1984). Dependence of the spectrum of Pc 3-4 pulsations on the interplanetary magnetic field. *Journal of Geophysical Research*, *89*(A5), 2770–2780. https://doi.org/10.1029/JA089iA05p02770

Torrence, C., & Compo, G. P. (1998). A practical guide to wavelet analysis. *Bulletin of the American Meteorological Society*, *79*, 61–78. https://doi.org/10.1175/1520-0477(1998)079<0061:APGTWA>2.0.CO;2

Turc, L., Escoubet, C. P., Fontaine, D., Kilpua, E. K. J., & Enestam, S. (2016). Cone angle control of the interaction of magnetic clouds with the Earth's bow shock. *Geophysical Research Letters*, *43*, 4781–4789. https://doi.org/10.1002/2016GL068818

Turc, L., Ganse, U., Pfau-Kempf, Y., Hoilijoki, S., Battarbee, M., Juusola, L., & Palmroth, M. (2018). Foreshock properties at typical and enhanced interplanetary magnetic field strengths: Results from hybrid-Vlasov simulations. *Journal of Geophysical Research: Space Physics*, *123*(0), 5476–5493. https://doi.org/10.1029/2018JA025466

von Alfthan, S., Pokhotelov, D., Kempf, Y., Hoilijoki, S., Honkonen, I., Sandroos, A., & Palmroth, M. (2014). Vlasiator: First global hybrid-Vlasov simulations of Earth's foreshock and magnetosheath. *Journal of Atmospheric and Solar-Terrestrial Physics*, *120*, 24–35. https://doi.org/10.1016/j.jastp.2014.08.012

Wilson, L. B. (2016). Low frequency waves at and upstream of collisionless shocks. *Washington DC American Geophysical Union Geophysical Monograph Series*, *216*, 269–291. https://doi.org/10.1002/9781119055006.ch16

Wu, M., Hao, Y., Lu, Q., Huang, C., Guo, F., & Wang, S. (2015). The role of large amplitude upstream low-frequency waves in the generation of superthermal ions at a quasi-parallel collisionless shock: Cluster observations. *Astrophysical Journal*, *808*, 2. https://doi.org/10.1088/0004-637X/808/1/2

Yermolaev, Y. I., Nikolaeva, N. S., Lodkina, I. G., & Yermolaev, M. Y. (2012). Geoeffectiveness and efficiency of CIR, sheath, and ICME in generation of magnetic storms. *Journal of Geophysical Research*, *117*, A00L07. https://doi.org/10.1029/2011JA017139